The Use of Multi-Scale Dimensionality Analysis for the Characterization of Debris Distribution Patterns

David A. Bonneau[1] and D. Jean Hutchinson[1]
[1] *Department of Geological Sciences and Geological Engineering - Queen's University, Kingston, Ontario, Canada*

ABSTRACT

A new methodology of linking grain size and debris movement is presented. A postglacial river terrace along the Thompson River has been monitored with terrestrial laser scanning and high resolution panoramic photographs for almost a 3-year study period. Multiscale Model to Model Cloud Comparison (M3C2) change detection and a multi-scale dimensionality analysis (CANUPO) have been performed to track the deposition patterns occurring in this active cliff talus system. The high resolution remote sensing data permitted us to link the geomorphic processes occurring along the cliff face with deposition and mass wasting events occurring on the talus slope. The detailed understanding of cliff processes gained, permits us to evaluate cliff retreat rates and the expected rate of deposition of material into the ditch along the railway track right of way at the base of the slope.

RÉSUMÉ

Une nouvelle méthodologie de liaison entre la taille des grains et le mouvement des débris est présentée. Une terrasse riveraine postglaciaire le long de la rivière Thompson a été surveillée au moyen d'un balayage laser terrestre et de photographies panoramiques à haute résolution pendant presque une période d'étude de trois ans. La détection de changement de modèle à échelle multi-échelle (M3C2) et une analyse de dimensionnalité à échelles multiples (CANUPO) ont été effectuées pour suivre les modèles de dépôt se produisant dans ce système actif de talus falaise. Les données de télédétection à haute résolution nous ont permis de relier les processus géomorphiques se produisant le long de la paroi de la falaise avec les événements de dépôt et de gaspillage de masse se produisant sur la pente du talus. La compréhension détaillée des processus de falaise acquise nous permet d'évaluer les taux de retrait des falaises et le taux prévu de dépôt de matériaux dans le fossé le long de l'emprise de la voie ferrée à la base de la pente.

1   INTRODUCTION

The Thompson River Valley, crosses the divide between the Coast Mountains and the Interior Plateau of British Columbia. The jagged glaciated Coast Mountains transition to the east to become the rolling hills of the Interior Plateau, which is interrupted by the deeply incised valley of the Thompson River. The Thompson valley was influenced by Pleistocene glaciation and thick Quaternary sediments are present (Church and Ryder 2010). A drift mantle of variable thickness covers level to moderately sloping upland areas (Ryder 1976, 1981). The glacial history in the Thompson Valley has had an impact on the occurrence of geohazards in this transportation corridor (Clague and Evans 2003).

The geohazards along the Thompson Valley have been a subject of research for the past number of decades. This can be attributed to the management of geohazards potentially affecting the Canadian Pacific (CP) and Canadian National (CN) rail lines and BC Highway 1 (BC 1) which follow the incised river valley to the confluence with the Fraser River. At several locations in the valley, the linear infrastructure is exposed to large rotational and retrogressive landslides. These landslides are confined to multiple glaciolacustrine clay-rich units, outwash sand and

gravel and boulder-rich till diamictons related to at least three Pleistocene glaciations (Clague and Evans 2003, Eshraghian 2007, Bishop 2008, Huntley and Bobrowsky 2014).

The CN rail line also traverses the base of the White Canyon, near the confluence of the Thompson and Fraser Rivers. The White Canyon, is an active section of CN's Ashcroft subdivision generating geohazards ranging from rockfalls to debris flows (Kromer et al. 2015, Bonneau and Hutchinson 2017, Rowe 2017, van Veen et al. 2017). As part of the Rail Ground Hazard Research Program (RGHRP), terrestrial laser scanning (TLS) has been completed at the White Canyon and several other sites in Thompson Valley since early 2012 (Gauthier et al. 2012).

Sandy Cobble Hill (SCH), a sequence of Quaternary sediments, has been monitored with TLS, aerial laser scanning and Structure-from-Motion photogrammetry with Multi-View-Stereo as a part of the RGHRP program by Queen's University. SCH is an active cliff-talus system in which erosion of the Quaternary valley fill sediments, has resulted in the formation of a steep gullied cliff face and talus slope accumulating debris in distinct patterns below. SCH represents a common landform in the Thompson River Valley (Ryder 1976, 1981). Both the CN and CP rail lines and BC 1 traverse the base of multiple of these types

of slopes throughout the river valley. The debris falling from the cliff face and the debris movement on the talus slope both present potential hazards to the linear infrastructure below. Therefore, gaining a thorough understanding of the geomorphic processes occurring in this cliff-talus system can help support mitigation and maintenance planning for operators of linear infrastructure in this transportation corridor.

The primary objective of this study is to present a methodology to aid in the understanding of geomorphic processes and depositional patterns occurring on cliff-talus systems, characterized using remote sensing technologies. This includes the implementation of a multi-scale dimensionality analysis technique (Brodu and Lague 2012) to track distributions of granular sediment on the talus slope. Although the study site does not present the largest geohazard to the rail track, this study represents a preliminary trial of the methodology on a slope with simple geometry. Proving the success of the method, this process can then be applied to debris channels and slopes with much more complex geometries to aid in our understanding of active processes occurring on those slopes and help mitigate future losses.

2   SITE LOCATION

Sandy Cobble Hill (SCH) is located along the CN main line in the Ashcroft subdivision (Mile 85.75 to 85.90). The slope is situated between Lytton and Spences Bridge, British Columbia; approximately 170 km northeast of Vancouver, British Columbia, Canada (Figure 1). The rail line is protected by a series of ditches, which accumulate debris originating from the steep cliff above the talus slope. The crest of the slope is approximately 120 m away from the track level.

Anderton (1970) mapped the study slope as a postglacial river terrace. Ryder (1981), later mapped the study site as a gullied river terrace with an alluvial fan (mudflow). The study slope consists of a sequence of unconsolidated Quaternary sediments. The approximately 20-meter-tall cliff face displays a sequence of well stratified and moderately well sorted gravel and sand (Figure 1). Both horizontal bedding and crossbedding can be seen, and these structures indicate that historical flow direction was in the same direction as the modern Thompson River. A series of horizontal unconformities within the gravels are marked by landslide deposits (Armstrong and Fulton, 1965; Anderton, 1970) and by cobble and boulder horizons (Ryder 1981). These occur between 43 and 60 m above present river level and constitute a terraced, erosional surface that was formed between two episodes of gravel deposition (Ryder, 1981). These fluvial gravels displayed at SCH, are referred to as the "Nicoamen gravels". The Nicoamen gravels are exposed in roadcuts and riverbanks from Botanie Creek to Seddall and lie between lower silt and an upper till (Anderton, 1970; Ryder, 1981). They are thought to have been deposited during the Olympia interglaciation (Ryder, 1981). The afore mentioned upper till unit consists of poorly sorted and non-sorted gravels containing till inclusions, this layer is up to 45 m in thickness near the Nicoamen River. Ryder (1981) interpreted this

material as advance outwash and other drift material from the Fraser Glaciation.
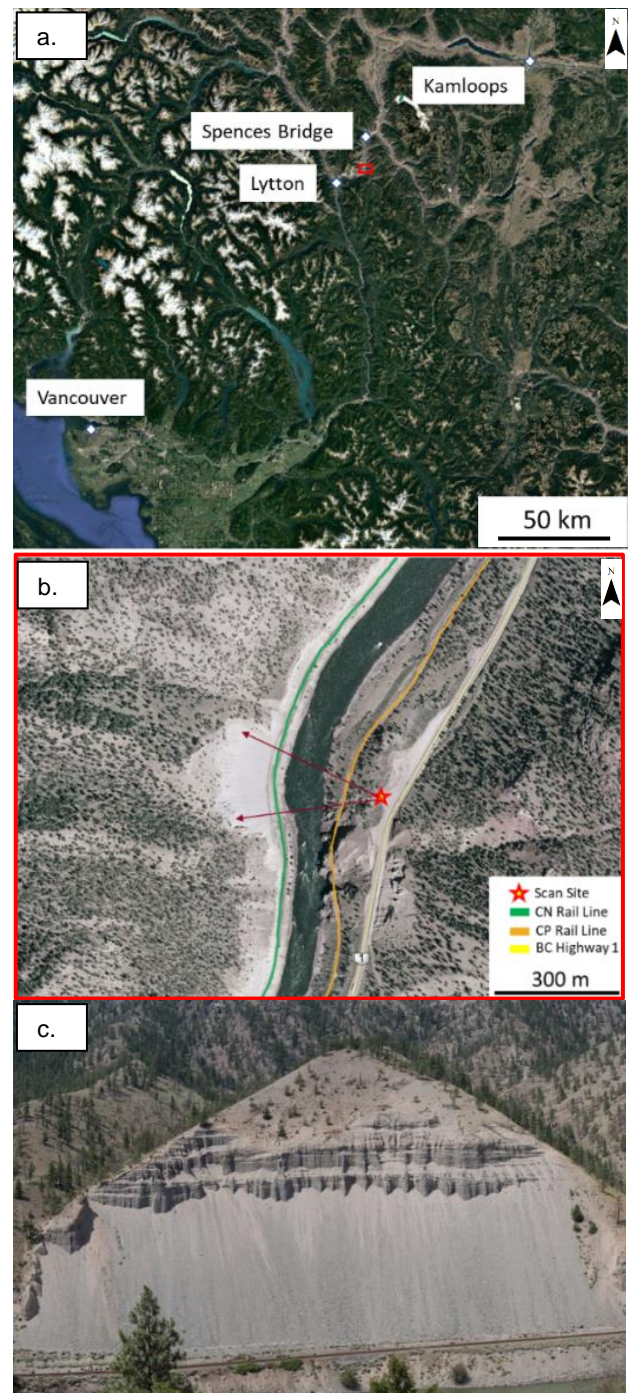
Figure 1. (a) Location of Sandy Cobble Hill and the surrounding terrain. (b) Displaying the scan location for all TLS acquisitions. (c) Looking directly east at the study slope.

3   METHODS

This section describes the data collection methods as well as the subsequent analytical methodology used in the study.

3.1   Terrestrial Laser Scanning (TLS)

An Optech Ilris 3D-ER terrestrial laser scanner was used to scan the study slope from the opposite bank of the Thompson River. The Optech Ilris 3D-ER is a time-of-flight TLS system which utilizes a 1,535 nm (infrared) wavelength.

For all TLS acquisitions, the slope was scanned from a single position, above the CP rail line next to BC 1 (Figure 1.b). The slope is approximately 375 meters away from this scan site. A single scan box was used to capture the entire slope. The vertical and horizontal angular resolution was set to 0.013 degrees for all scans. This resulted in an approximate point spacing of 8 centimeters across the slope.

For this study, thirteen TLS scans were analyzed. The baseline scan for this study was taken on November 5th, 2014. The last scan used in this study was captured on September 1st, 2017. Scans were typically taken approximately every three months.

3.2   High Resolution Panoramic Photographs

High resolution panoramic photographs of the slope were collected using a 36-megapixel Nikon D800 full-frame DSLR camera, equipped with a Nikkor 135 mm f/2 prime lens and a global positioning system (GPS). The camera was attached to a GigaPan robotic head mounted to a tripod. The GigaPan head was used to ensure 60% overlap in the images. Approximately 100 photographs were taken from the same site from which the TLS scan was taken. The photographs were then stitched together using GigaPan's Stitch software to create a panoramic image. These panorama images are used to permit visual inspection of the slope, verification of change. Additionally, the panoramic images were used to track detached cobbles from the cliff.

3.3   Point Cloud Registration

Each TLS data set was registered in CloudCompare. This was accomplished in a two-step process. An initial alignment was completed by point picking common geometric features in both data sets (Oppikofer et al. 2009, Kromer et al. 2015, van Veen et al. 2017). Once the point cloud has been roughly aligned, an iterative closest point algorithm was then applied to refine the initial alignment (Besl and McKay 1992).

3.4   Change Detection Methodology

Multiscale Model to Model Cloud Comparison (M3C2), was used to preform change detection between the subsequent TLS datasets of the study slope. Lague et al. (2013) provides a detailed overview of the change detection methodology.

The limit of detection for the change detection analysis was established by first determining the registration error in the alignment process. The mean alignment standard deviation for the approximately 8 cm point spacing data, was 0.012 m, which is consistent with the instrumental error (or noise). This was then incorporated in the M3C2 distance calculations (Lague et al. 2013).

3.5   2.5D Volume Calculations

All volume calculations were completed in CloudCompare. To compute the volume, CloudCompare first generates rasters in a user defined projection direction. After this is completed, the contributions of each cell are summed together. The contribution is the volume, corresponding to the cell footprint multiplied by the difference in heights. To calculate the volumes, areas of change were first segmented out using the segmentation tool. The area of change was translated to align with one of the principal axes. This ensured that the projection direction would correspond to the change direction. This ensured that the projection direction would not over or underestimate the volume.

3.6   CAractérisation de NUages de POints (CANUPO)

CAractérisation de NUages de POints (CANUPO) is a multi-scale dimensionality classification technique developed by Brodu and Lague (2012). This is a semi-supervised machine learning technique which operates directly on the point cloud and is based solely on the point cloud geometry. For further details on the CANUPO methodology, readers are referred to Brodu and Lague (2012).

In this study, CANUPO was used to remove vegetation and to classify the debris accumulations on the talus slope into two grain size bins. Both processes were completed using the CANUPO implementation in CloudCompare. The grain size classification aimed to identify the boulder sized blocks (> 0.256 m diameter - Wentworth 1922) on the talus slope. The largest grain size was first identified using a combination of the TLS and the panoramic photography.

An example of the results of the classification for a TLS scan from June 2015 can be seen in Figure 2. This classifier was applied to all TLS scans. Verification of the classification was confirmed manually by measuring visible particles in the TLS point clouds and counting pixels in the panoramic photographs.

4   RESULTS

Over the course of the approximately 2 years and 10-month study period, a significant amount of change has occurred in the cliff face (Figure 3). Failure appears to be concentrated in a lower cobble layer; in addition to another concentration of failure in the southern most section of the cliff face. It should be noted that the cliff face in this section has a northeast aspect, while the rest of the cliff is predominantly east facing. All failure events captured with the M3C2 change detection could be confirmed with the panoramic photography.
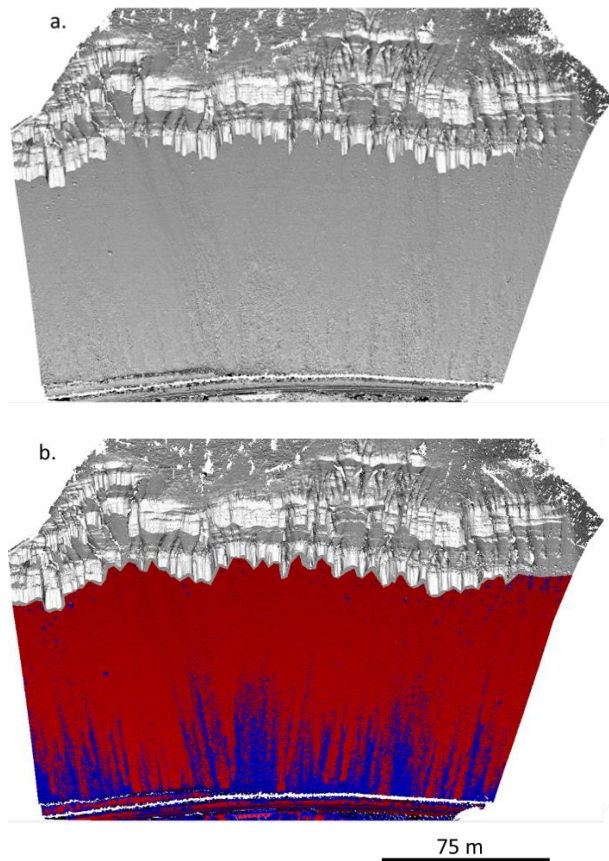
Figure 2. Oblique view of the TLS scene. (a) unclassified TLS point cloud. (b) classified TLS point cloud. Red represents areas on the slope with grain sizes below 25 cm in diameter. Blue represents areas on the slope with grain sizes above 25 cm in diameter. Note the classifier could identify fallen boulders and cobbles directly below the cliff.

The greatest amount of change appears to occur over the winter months (i.e. October to February). This is typically when the Thompson River valley receives the greatest amount of precipitation (Environment Canada, 2017). Visible surficial water erosion was noticeable in the panoramic photographs on the benches within the cliff face during February site visits. Figure 3.c, illustrates the distribution of failure over the winter months. Failure is concentrated in the lower cobble layer and at the interface between the Nicoamen gravels and colluvial soil on top of the cliff. It appears as if the slope change over the first winter (i.e. between 2014-11-05 and 2015-02-21) is largely concentrated in the lower cobble layer, while during the subsequent winters more failure is occurring in the upper interface.

The stability of the cliff appears to be strongly influenced by the cobble and gravel beds. Cross sections (Figure 4) through a section of the cliff face, indicate the cliff face is continuing to retrogress. For the specific area shown in Figure 4, the cliff has retreated approximately 1.75 m. This corresponds to approximately 0.62 m/year in

valley parallel retreat. It appears that the greatest amount of retrogression occurs during the winter months (Figure 4). The area along the cross section was mapped into three size classifications based on the primary particle size in a specific bed. The three mapped classes were: cobbles, gravel and sand. The panoramic photography of the cliff face, were used to visually map the particle sizes. Volume calculations were then preformed for the failure sequence for all the scan dates. The volume estimates were then tied back to the particle size mapping.

For the following TLS change detection figure, areas of grey signify locations where either no change has occurred or the change is smaller than the limit of detection. Negative change or areas of loss on the slope are denoted by a gradation from blue to purple.

Within the time-period analyzed, it was possible to track individual cobbles as they detached from the cliff face and were deposited on the slope below. 94 individual cobbles ranging in size from approximately 0.01 m^3 to 0.1 m^3, could be detected in the M3C2 change detection and with visual verification in the panoramic photographs. Only primary rockfall events (initial detachment) were considered for this analysis. It should be noted that 86 of the 94 cobbles which were able to be tracked all originated from the lower cobble layer in the cliff face.

The majority of the cobbles detaching from the cliff face are deposited in close proximity to the cliff face. 20 of the 94 cobbles came to rest 7.5 to 10 meters away from the slope. Only 4 of the 94 cobbles are transported further than 40 meters away from the cliff face. These correspond to the largest cobbles and boulders by volume which were detached. This aligns with previous studies of rockfall talus systems, in which the largest blocks typically have the highest momentum allowing the furthest runout distance

The M3C2 change detection provided insight in the initiation zones of debris movements occurring in the talus. In this study, it was found that of the 94 tracked cobbles which failed, none of these failure events appear to correspond to initiation locations of debris movements. As a result, the potential triggering mechanism for these events could correspond to oversteepening of the debris, overloading or even wildlife crossing the talus slope.

It appears there is a relationship between the deposition location of the flows and the coarsest fraction of grain sizes on the slope. This is illustrated with the CANUPO classification. Figure 5, displays this relationship. As it can be seen, the deposition area of the lobes appears stop in the areas which were classified greater than 25 cm in diameter in both TLS scans (purple). The areas of change in the classification are noted in green. Interestingly, in many of the lobes, a change in the grain size (green), occurs on the fringes of the deposit. This can be interpreted as the lateral and longitudinal sorting which is known to occur in this process.This implies that the classifier is can be used to detect the coarsest grain sizes on the boundaries of the lobe. Another finding and displayed in Figure 5, is the upward building progression of the deposits as they reach the ditch level. Over time, the deposits build and increases in higher elevation up slope. These continue to propagate up slope and eventually collapse. This sequence can be seen in the TLS change detection in Figure 5.
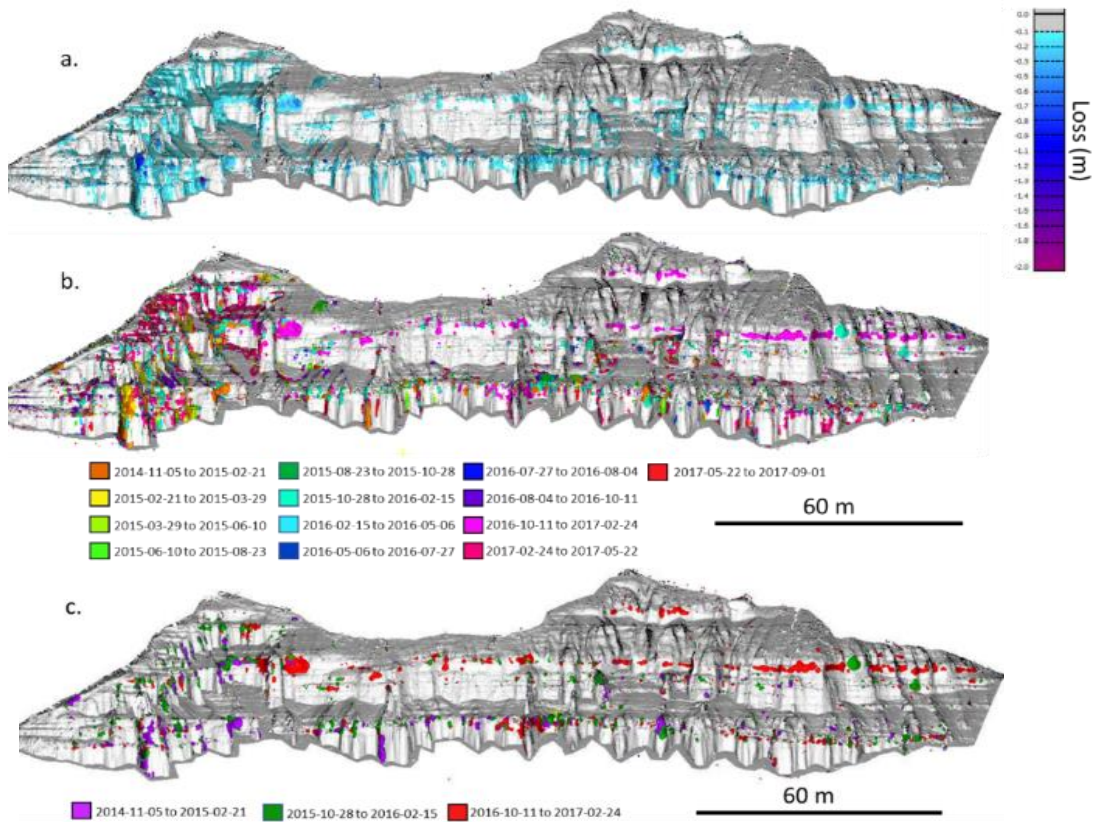
Figure 3. (a) Displaying all the negative change occurring in the cliff face. (b) Displaying all the negative change occurring in the cliff face broken in to time periods corresponding to TLS acquisition dates. (c) Displaying all the negative change occurring in the cliff face broken in to time periods corresponding to TLS acquisition dates over the winter months.
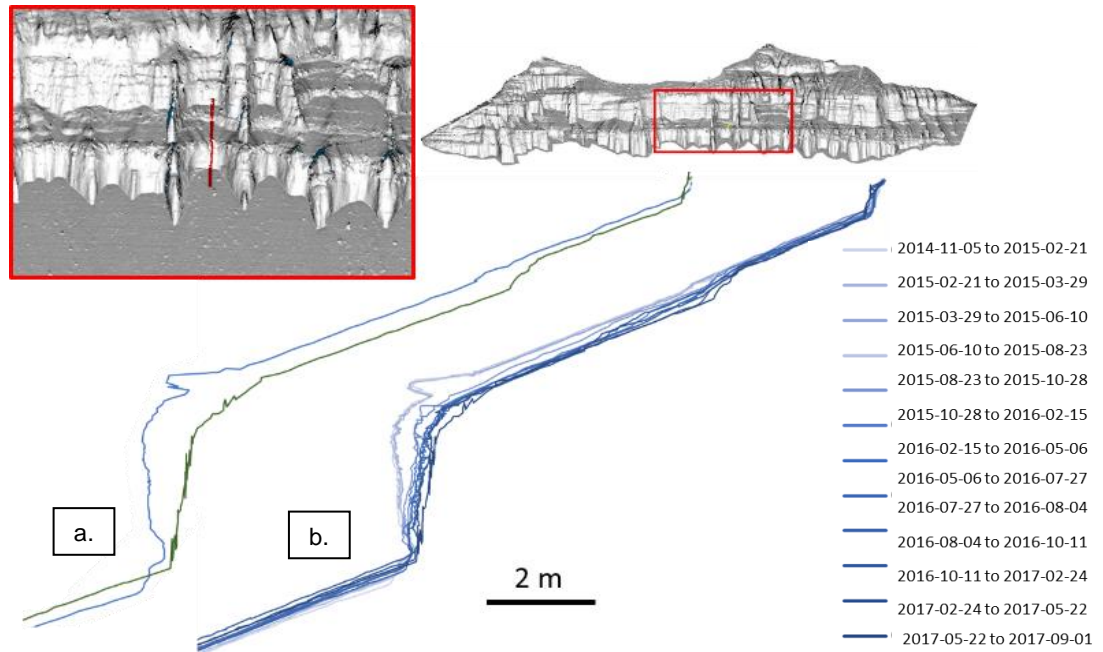
Figure 4. Cross sections through the cliff face at different times. The location of the cross section is shown as the red line in the inset image. (a) cross sections correspond to the first (blue) and last scan (green) dates. (b) cross sections for all the scan dates to display the progression of cliff failure.
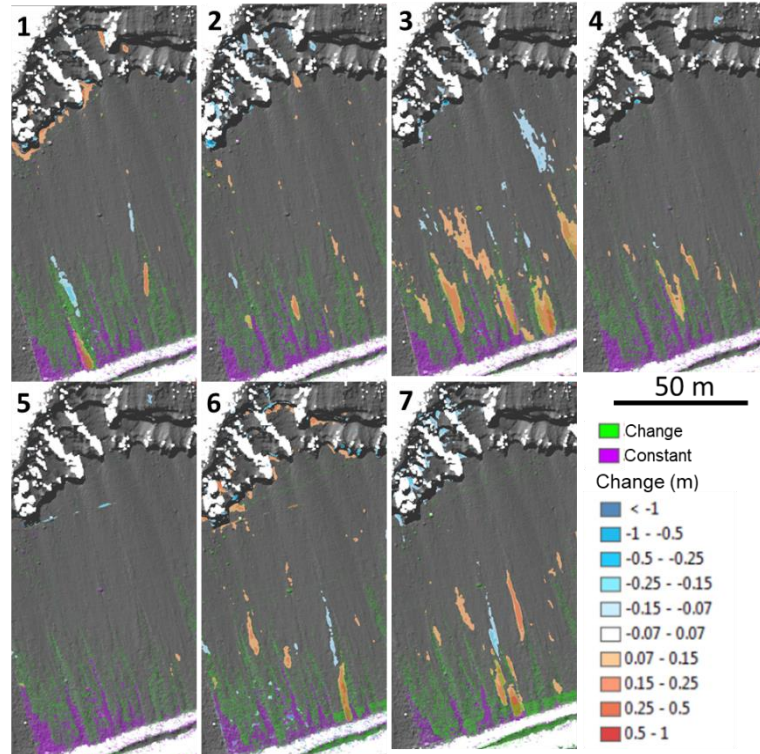
Figure 5. Displaying a time series of the distribution of particles sizes above 25 cm in diameter integrated with the M3C2 change detection. Purple denotes areas where the CANUPO classification of particles greater than 25 cm is constant between scans. Green represent represents areas of change in the particle distribution. (1) corresponds to the time period between the baseline scan and the next subsequent scan (2015-02-21). The increasing numbers correspond to the next change set between the next set of scan dates (ie. 2015-02-21 to 2015-03-29 = 2).

5. DISCUSSION

The mechanical processes underlying rockfall events have been the focus of a number of investigations (Dorren 2003 – review paper, see references within), while other studies have quantified local rockwall retreat rates based on talus volumes (e.g., Hales and Roering 2005, Sass 2006, Sass and Krautblatter 2007, Moore et al. 2009, Thapa et al. 2017). In this study, by utilizing high resolution remote sensing data, there is the ability to document the geomorphic processes occurring both in the cliff face and on the talus slope.

In this study, valley parallel retreat (Obanawa and Matsukura 2006) in the cliff face was captured with TLS change detection. The high-resolution TLS datasets provided a basis on which both the rate and spatial distribution of retreat were able to be captured. From the analysis, the stability of the cliff appears to be largely controlled by the cobble and gravel layers. Each significant retreat, occurs during the winter time. This could be a result of surface water erosion on the cliff face, which could have triggered the release of boulders and cobbles from the lower layer. A process which has been described by Dorren (2003).

The ability to track cobbles after detachment from the cliff-face can help in the understanding of the coupling relationship between rockfall and the initiation of mass wasting on the talus slope below. In this study there was success in tracking a great number of the cobbles and boulders which have detached from the cliff face. However not all cobbles which were released from the cliff face were able to be tracked. Cobbles which could not be tracked could have disappeared from the talus surface due to the sieving effect when they moved downslope into areas of coarser debris (Pérez 1985). Additionally, they could have come to rest in the ditch protecting the rail line, which is occluded from the vantage point where the TLS scans were taken.

The dominant mass wasting process occurring on the talus slope appears to be flows of debris. The deposits of the flows occurring at SCH follow previous descriptions of this mass wasting phenomena. These could be potentially interpreted as dry granular flows. In this context, they are defined as clasts that move under dry conditions (i.e. without ice coatings around the particles) and are deposited because of inter-particle friction acting on individual grains (Rapp 1960). Within all recorded debris movements at SCH, the threefold segregation of grain sizes (Van Steijn et al., 1995) can be seen in the panoramic photographs. The coarsest clasts are concentrated front of

the lobe, while smaller grains (fine gravel, coarse sand) form the tail of the flow. Both longitudinal and lateral sorting are visible in the deposits. There were also no levees seen in the change detection in the areas of movement. The initiation zones of the debris movements were not limited to the upper areas of the talus slope, contrary to previous studies on other slopes (Rapp, 1960; Van Steijn et al., 1995). The distribution of initiation zones varied across the slope. However, consistent with previous studies were that the majority of the movements only affected a shallow surficial layer in the talus. This is consistent with the findings of Pérez (1985) and van Steijn et al. (2002), who observed that grain flows occur only on slopes at or near the angle of repose for the material, and generally have a thickness of less than 5 cm. In the event occurring in at SCH, the depth varied between 5 cm up to approximately 30 cm in the largest recorded events. It is difficult to assess the influence of water in these events since the deposit could have been wetted during a previous precipitation event and dried out by the time of the observations.

The methodology of linking grain size and debris movements on a slope with simple geometry was presented here was found to be successful. The ability to semi-automatically identify the coarsest grains on the slope could be applied to other studies such as geomorphic mapping of debris flow fans, where the identification of stoney lobes from debris flows can be a crucial element in a debris flow risk assessment (Jakob et al. 2016). During a debris flow, channel avulsion can occur (de Haas et al. 2017); this is when a debris flow migrates from its main channel and can erode and entrain material in a different portion of the fan. Therefore, being able to systematically map locations where historical debris flow deposits, such as the afore mentioned stoney lobes can be found, can help our understanding of the debris flow phenomenon. Furthermore, the composition of a debris flow can significantly alter its flow rheology and resulting runout distance (de Haas et al. 2015). Therefore, understanding the distribution, size and shape of the material that could potentially be entrained could potentially provide estimates of runout potential of debris flows.

5   CONCLUSION

SCH represents an active cliff-talus system that is continuing to retrogress thereby subjecting the slope above the rail line to rockfall and dry granular flow hazards. These dissected postglacial river terraces are a common landform in the Thompson Valley. During this study, it was found that the use of both TLS and panoramic photography techniques supplement our understanding of slope processes which can be incorporated into hazard assessments and maintenance planning. High resolution photography was found to be a vital tool for visually confirming the fluxes within the talus deposits.

The ability to monitor the accumulation and debris distribution patterns across the entire slope will permit the estimation of expected volumes of debris which could eventually fail and impact the underlying rail line. The retreat rates calculated at the cliff face can be tied directly to expected volumes of debris which will be transported downslope. Operators of linear infrastructure in this transportation corridor can use this information to inform maintenance planning.

This study has shown the successful implementation of a methodology which can be used to start to link debris movement with grain size. The next steps are to begin to explore the applicability of this methodology to slopes with a more complex slope geometry.

REFERENCES

Anderton, L.J. 1970. Quaternary Stratigraphy and Geomorphology of the Lower Thompson Valley, British Columbia. MSc. Thesis. University of British Columbia.

Besl, P., and McKay, N. 1992. A Method for Registration of 3-D Shapes. doi:10.1109/34.121791.

Bishop, N.F. 2008. Geotechnics and hydrology of landslides in Thompson River Valley, near Ashcroft, British Columba. : 117.

Bonneau, D.A., and Hutchinson, D.J. 2017. Applications of Remote Sensing for Characterizing Debris Channel Processes. *In* Landslides: Putting Experience, Knowledge and Emerging Technologies into Practice. *Edited by* J. V. De Graff and A. Shakoor. Association of Environmental & Engineering Geologists (AEG), Roanoke, USA. pp. 748–759.

Brodu, N., and Lague, D. 2012. 3D terrestrial lidar data classification of complex natural scenes using a multi-scale dimensionality criterion: Applications in geomorphology. ISPRS Journal of Photogrammetry and Remote Sensing, **68**(1): 121–134. International Society for Photogrammetry and Remote Sensing, Inc. (ISPRS). doi:10.1016/j.isprsjprs.2012.01.006.

Church, M., and Ryder, J. 2010. Physiography of British Columbia. *In* Compendium of Forest Hydrology and Geomorphology in British Columbia. *Edited by* R.G. Pike, T.E. Redding, R.D. Moore, R.D. Winker, and K.D. Bladon. Kamloops, BC. pp. 17–46.

Clague, J.J., and Evans, S.G. 2003. Geologic framework of large historic landslides in Thompson River Valley, British Columbia. Environmental and Engineering Geoscience, **9**(3): 201–212. doi:10.2113/9.3.201.

Dorren, L.K.A. 2003. A review of rockfall mechanics and modelling approaches. Progress in Physical Geography, **27**(1): 69–87. doi:10.1191/0309133303pp359ra.

Eshraghian, A. 2007. Hazard Analysis of Reactivated Earth Slides in the Thompson River Valley , Ashcroft , British Columbia. University of Alberta.

Gauthier, D., Lato, M., Edwards, T., and Hutchinson, D.J. 2012. Rockfall and Talus Accumulation From Serial LiDAR Scans: a Railway Case Study From the White

Canyon, Thompson River, BC. *In* GeoManitoba.

de Haas, T., Braat, L., Leuven, J.R.F.W., Lokhorst, I.R., and Kleinhans, M.G. 2015. Effects of debris flow composition on runout, depositional mechanisms, and deposit morphology in laboratory experiments. Journal of Geophysical Research F: Earth Surface, **120**(9): 1949–1972. doi:10.1002/2015JF003525.

de Haas, T., Densmore, A.L., Stoffel, M., Suwa, H., Imaizumi, F., Ballesteros-Cánovas, J.A., and Wasklewicz, T. 2017. Avulsions and the spatio-temporal evolution of debris-flow fans. Earth-Science Reviews, **177**(November): 53–75. Elsevier. doi:10.1016/j.earscirev.2017.11.007.

Hales, T.C., and Roering, J.J. 2005. Climate-controlled variations in scree production, Southern Alps, New Zealand. Geology, **33**(9): 701. doi:10.1130/G21528.1.

Huntley, D.H., and Bobrowsky, P.T. 2014. Surficial geology and monitoring of the Ripley Slide, near Ashcroft, British Columbia, Canada. Geological Survey of Canada, **Open Fiile**. doi:10.4095/293453.

Jakob, M., Holm, K., and McDougall, S. 2016. Debris-Flow Risk Assessment. Oxford University Press USA. doi:10.1093/acrefore/9780199389407.013.37.

Kromer, R.A., Hutchinson, D.J., Lato, M.J., Gauthier, D., and Edwards, T. 2015. Identifying rock slope failure precursors using LiDAR for transportation corridor hazard management. Engineering Geology, **195**: 93–103. Elsevier B.V. doi:10.1016/j.enggeo.2015.05.012.

Lague, D., Brodu, N., and Leroux, J. 2013. Accurate 3D comparison of complex topography with terrestrial laser scanner: Application to the Rangitikei canyon (N-Z). ISPRS Journal of Photogrammetry and Remote Sensing, **82**: 10–26. International Society for Photogrammetry and Remote Sensing, Inc. (ISPRS). doi:10.1016/j.isprsjprs.2013.04.009.

Moore, J.R., Sanders, J.W., Dietrich, W.E., and Glaser, S.D. 2009. Influence of rock mass strength on the erosion rate of alpine cliffs. Earth Surface Processes and Landforms, **34**(10): 1339–1352. doi:10.1002/esp.1821.

Obanawa, H., and Matsukura, Y. 2006. Mathematical modeling of talus development. Computers and Geosciences, **32**(9): 1461–1478. doi:10.1016/j.cageo.2006.05.004.

Oppikofer, T., Jaboyedoff, M., Blikra, L., Derron, M.-H., and Metzger, R. 2009. Characterization and monitoring of the Åknes rockslide using terrestrial laser scanning. Natural Hazards and Earth System Science, **9**(3): 1003–1019. doi:10.5194/nhess-9-1003-2009.

Pérez, F.L. 1985. Surficial Talus Movement in an Andean Paramo of Venezuela. Geografiska Annaler. Series A, Physical Geography, **67**(3): 221–237.

Rowe, E.M. 2017. An examination of structural constraints on rockfall behaviour using LiDAR data. Queen's University.

Ryder, J.M. 1976. Terrain Inventory and Quaternary Geology, Ashscroft, British Columbia. Geological Survey of Canada, **74–49**: 1–17. Department of Energy, Mines and Resources, Ottawa, Ontario.

Ryder, J.M. 1981. Terrain Inventory and Quaternary Geology, Lytton, Biritsh Columbia. Geological Survey Paper, **79–25**: 1–20.

Sass, O. 2006. Determination of the internal structure of alpine talus deposits using different geophysical methods (Lechtaler Alps, Austria). Geomorphology, **80**(1–2): 45–58. doi:10.1016/j.geomorph.2005.09.006.

Sass, O., and Krautblatter, M. 2007. Debris flow-dominated and rockfall-dominated talus slopes: Genetic models derived from GPR measurements. Geomorphology, **86**(1–2): 176–192. doi:10.1016/j.geomorph.2006.08.012.

van Steijn, H., Boelhouwers, J., Harris, S., and Hétu, B. 2002. Recent research on the nature, origin and climatic relations of blocky and stratified slope deposits. Progress in Physical Geography, **26**(4): 551–575. doi:10.1191/0309133302pp352ra.

Thapa, P., Martin, Y.E., and Johnson, E.A. 2017. Quantification of controls on regional rockfall activity and talus deposition, Kananaskis, Canadian Rockies. Geomorphology, **299**: 107–123. Elsevier B.V. doi:10.1016/j.geomorph.2017.09.039.

van Veen, M., Hutchinson, D.J., Kromer, R., Lato, M., and Edwards, T. 2017. Effects of sampling interval on the frequency - magnitude relationship of rockfalls detected from terrestrial laser scanning using semi-automated methods. Landslides, (January): 1–14. Landslides. doi:10.1007/s10346-017-0801-3.

Wentworth, C.K. 1922. A Scale of Grade and Class Terms for Clastic Sediments. The Journal of Geology, **30**(5): 377–392.